Numerical analysis of effect of temperature history and restraint degree on cracking behavior of early-age concrete

Jianda Xin*,**, Guoxin Zhang*,**, Yi Liu*,**, Zhenhong Wang*,** and Zhe Wu*,**

*State Key Laboratory of Simulation and Regulation of Water Cycle in River Basin, China Institute of Water Resources and Hydropower Research, Beijing 100038, P. R. China
**Department of Structures and Materials, China Institute of Water Resources and Hydropower Research, Beijing 100038, P. R. China
Corresponding Author: zhanggx@iwhr.com

Submitted: 10/07/2018
Revised: 28/10/2018
Accepted: 13/11/2018

ABSTRACT

This paper presents a numerical analysis of concrete restraint tests conducted on a temperature stress testing machine (TSTM). Two numerical methods, namely, 1D method using Matlab software and 3D method using Midas software, were adopted. Factors, such as cooling rate and external restraint degree, were numerically analyzed and compared with experimental results. Results show that numerical analyses of concrete restrained stresses were comparable with those of TSTM tests. The cracking potential of concrete decreased with higher cooling rate at early age, and this benefit became more considerable for concrete structures under higher external restraint conditions. A simplified relationship between the external restraint degree and the allowed temperature difference (the difference between maximum temperature and cracking temperature of concrete) is developed. Furthermore, it is found that the anti-cracking capability of concrete under different restraint conditions can be overestimated up to 56% when ignoring creep effect on values of restraint degree.

Keywords: Concrete cooling rate; Early-age; Concrete cracking; TSTM tests; Numerical analysis; RC restraint degree.

INTRODUCTION

Due to the hydration of cement, considerable heat can be generated after concrete casting, which is an essential issue for the massive concrete structure construction. Usually, the temperature inside during the initial concrete hydration process can reach 60°C and the subsequent thermal deformation is not negligible (Zhu, 2013). Stresses are generated once these deformations are restrained. Creep of concrete is another time-dependent behavior under long-term loading and is important for estimation of restrained stress. Due to the high creep deformation, the concrete tensile stress can be greatly reduced and the potential of concrete cracking is lowered (Hossain and Weiss, 2004).

Once the tensile stress in concrete exceeds its tensile strength, crack will occur (Khan et al., 2017; Altoubat et al., 2017; Kovler and Bentur, 2009). Cracking of massive concrete structures has drawn much attention since the tensile strength of concrete is relatively weak. The cracking resistance of concrete is influenced by many factors, such as autogenous shrinkage, hydration heat, creep, mechanical property, and restraint degree (Lee et al., 2003; Amin et al., 2009; Fan et al., 2015). In particular, thermal deformation (caused by the hydration heat) and external restraint (caused by the foundation and/or adjoining structures) are two important factors that affect restrained stress

magnitude of massive concrete structures (Emborg, 1989; Altoubat et al., 2016). Usually, large temperature difference and high restraint degree will exacerbate the evolution of restrained stress (Wang et al., 2015; Hossain and Weiss, 2004; Breitenbücher, 1990). Several restraint tests, such as ring (Altoubat et al., 2017; Altoubat et al., 2016; Hossain and Weiss, 2004), slab (Wang et al., 2017), and linear specimens (Kovler and Bentur, 2009; Amin et al., 2009; Breitenbücher, 1990), have been developed to investigate restrained stress and cracking behavior of concrete.

For example, for restrained ring tests, strain gages were adhered in the inner side of steel ring and collected data can be used for calculation of restrained stress of concrete, as well as cracking potential evaluation (Hossain and Weiss, 2004). For restrained cracking frame tests, strain gages were adhered on the steel frame, then the stress evolution of concrete can be calculated based on principles of deformation compatibility and force equilibrium (Breitenbücher, 1990).

Recently, a series of restraint tests have been conducted by the researchers using a temperature stress testing machine (TSTM) and the effects of cooling rate and restraint degree on restrained stress of concrete have been investigated (Zhang and Qin, 2006; Shi et al., 2014). Nevertheless, during the early-age stage of concrete after casting, many phenomena, such as mechanical properties, creep, temperature history, and external restraint condition, occur simultaneously and complex the understanding of restrained stress evolution and cracking behavior of concrete.

The aim of this paper is to numerically analyze the effect of cooling rate and restraint degree on cracking behavior of concrete. The experiment details and results of TSTM tests were firstly overviewed. Then, a 1D method using Matlab software and a 3D method using Midas software were employed to numerically calculate and verify the experimental results of concrete restraint tests. Finally, the calculated results of the two numerical methods were compared and discussed with experimental data.

DETAILS AND RESULTS OF TSTM TESTS

Test details

The concrete mixtures were made of ordinary Portland cement, fly ash, natural sand, and crushed stone with a maximum particle size of 40 mm. The water-to-binder ratio for the concrete mixture was 0.5 and the slump value was 40~60mm. Table 1 shows the mixture proportions of concrete.

Table 1. Mixture proportions of concrete (kg/m^3).

Concrete grade	Cement	Water	Fly ash	Sand	Gravel	Water reducer	Air-entraining admixture	Compressive strength at 28 day (MPa)
C20	108	83	58	539	1776	0.996	0.02656	24.4

The specimen was designed to go through a three-phase temperature variation (Fig. 1): a semi-adiabatic temperature phase, a fast cooling temperature phase, and a slow cooling temperature phase. The cooling temperature phase lasted until the concrete cracked.

Two temperature histories and three restraint degrees (100%, 75%, and 50%) for concrete specimens were selected.

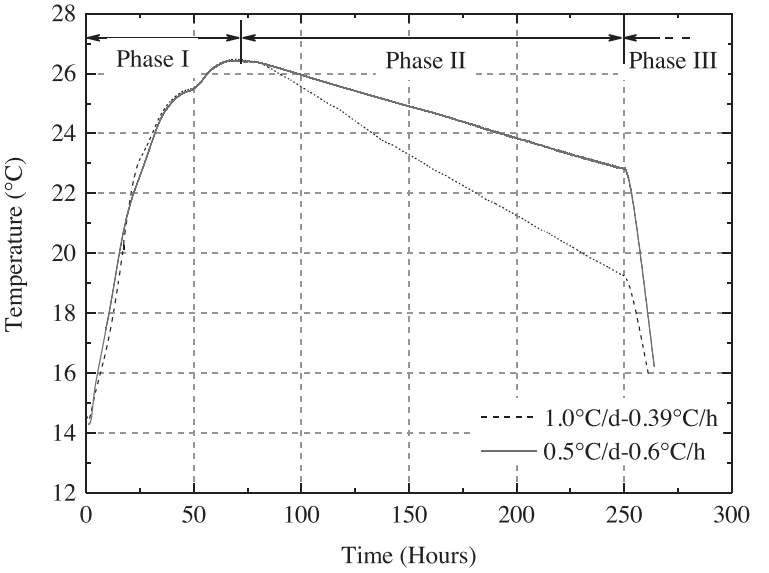

Figure 1. Temperature histories of concrete specimens.

A temperature stress testing machine (TSTM), which was firstly developed by Springenschmid et al. (1994), then improved by others (Kovler, 1994; Lin, 2006), was employed in the current research. Two specimens with identical dimensions (shown in Fig. 2) are simultaneously cast. One of them (free specimen) is free to deform during the test and the other (restrained specimen) is loaded through a gripped end under a certain restraint degree. The deformation of specimen can be collected by a linear variable differential transformer (LVDT) mounted on the end of quartz rod, which synchronously moves with specimen. The restrained stress induced by a motor is recorded by a load cell. Signals from thermometers, LVDTs, and load cell are transferred through an amplifier to the computer for calculations of corresponding temperature, deformation, and force value. The photo of this device is shown in Fig. 3.

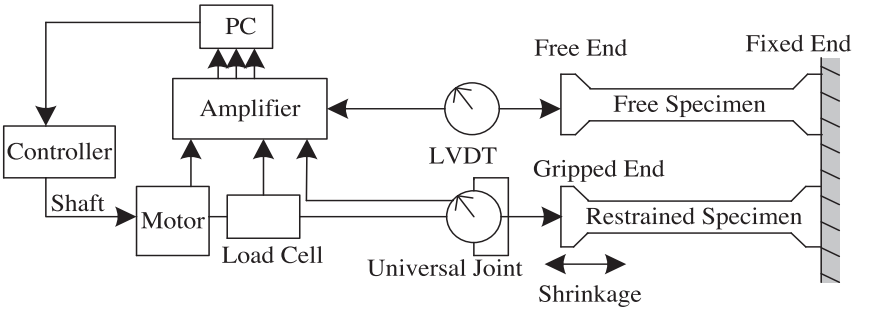

Figure 2. Schematic description of the closed loop instrumented restraining system (Springenschmid et al., 1994).

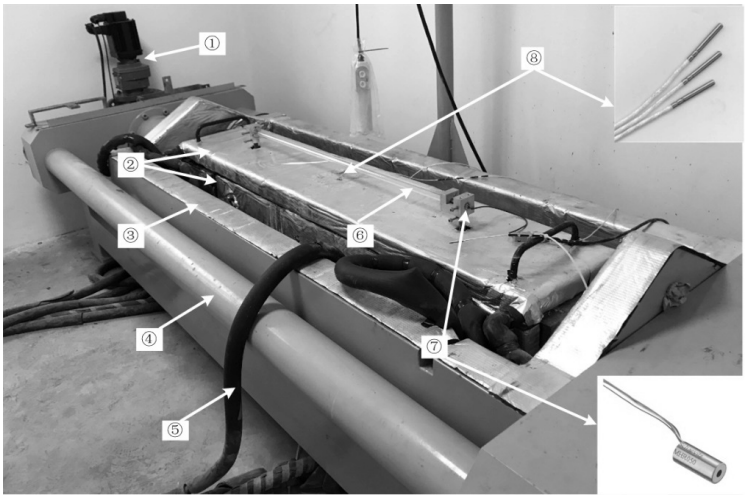

① Motor; ② Temperature controlling mold; ③ Thermal insulation box; ④ Reaction frame; ⑤ Circulating pipe; ⑥ Quartz rod; ⑦ LVDT; ⑧ Thermometer

Figure 3. Photo of TSTM.

The degree of restraint γ_R in TSTM tests is defined as (Zhang and Qin, 2006)

$$\gamma_R = \frac{\varepsilon^{fr} - \varepsilon^{res}}{\varepsilon^{fr}} \quad (1)$$

where ε^{fr} is the free deformation of concrete; ε^{res} is the residual deformation of restrained concrete.

Eq. (1) can also be rewritten as

$$\varepsilon^{res} = (1-\gamma_R)\varepsilon^{fr} \quad (2)$$

When the restraint degree γ_R is chosen, ε^{res} of restrained specimen calculated by Eq. (2) then can be controlled by a servo motor.

Fig. 4 shows a typical deformation curve of TSTM restrained specimen. Under 100% restraint degree condition, once the deformation of specimen reached a threshold value, the motor was activated to push/pull the specimen to specific positions.

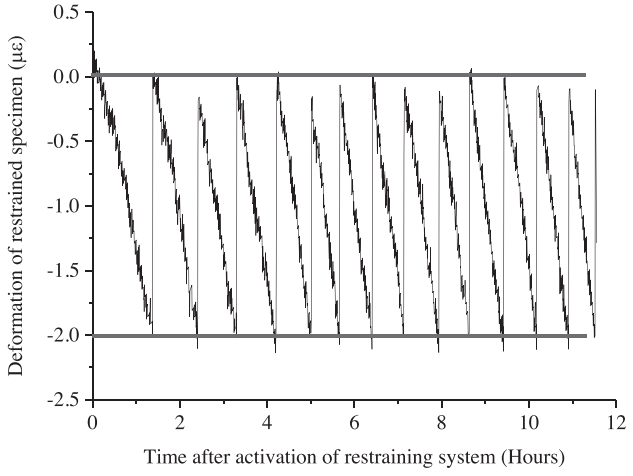

Figure 4. Typical deformation curve of TSTM restrained specimen (100% restraint degree).

Fig. 5 shows the dimensions of TSTM specimen.

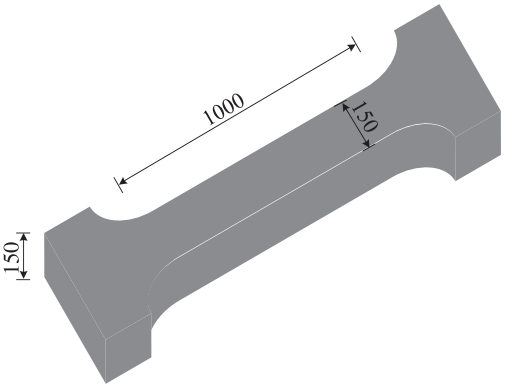

Figure 5. Dimensions of TSTM specimen (Unit: mm).

Crack of concrete specimen is shown in Fig. 6.

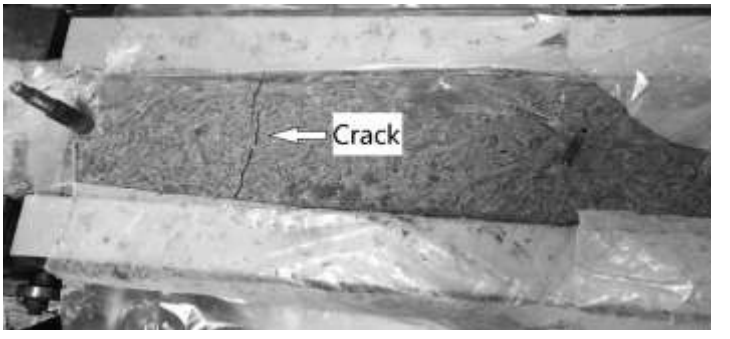

Figure 6. Crack of TSTM specimen.

Experimental results

The mechanical properties of concrete mixtures were tested according to the Chinese code GB/T50081-2002 (2002); the dimensions are 100 mm × 100 mm × 300 mm (prism specimen for elastic modulus test) and 100mm × 100mm × 100mm (cube specimen for splitting tensile strength test).

The relationship between the elastic modulus and the age can be expressed as (Zhu, 2013)

$$E(t) = E_{28}[1 - \exp(-at^b)] \quad (3)$$

where E_{28} is the elastic modulus of concrete at 28 days, a and b are constants depicting evolution trends of concrete mechanical properties, which can be determined from the experimental data, and t is the concrete age.

Based on experimental data, the optimally approximated values of E_{28}, a and b were 36.8, 0.31, and 0.83, respectively.

Similarly, the evolution of splitting tensile strength of concrete shared a similar trend with that of elastic modulus. The relationship between the splitting tensile strength and the age can be expressed by Eq. (4) (Zhu, 2013).

$$f_{sp}(t) = f_{sp,28}[1 - \exp(-at^b)] \quad (4)$$

where $f_{sp,28}$ is the splitting tensile strength of concrete at 28 days.

The optimally approximated values of $f_{sp,28}$, a and b were 1.98, 0.08, and 1.37, respectively.

The coefficient of thermal expansion (CTE) of concrete was tested based on the free deformation induced by a temperature history ranging from 21°C-29°C and the calculated value was approximately 7.5με/°C.

Fig. 7 (a) and (b) show the evolutions of restrained stress of concrete under different cooling histories and restraint degrees.

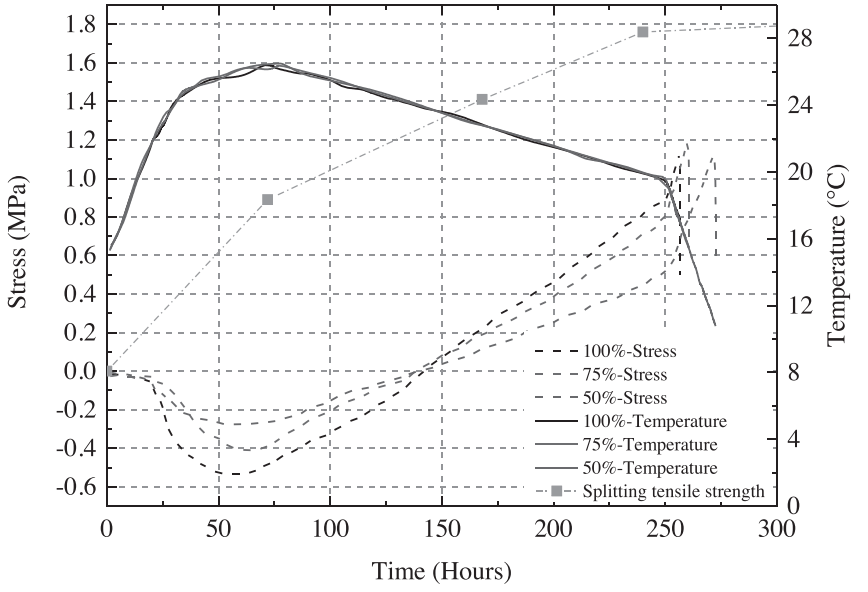

(a)

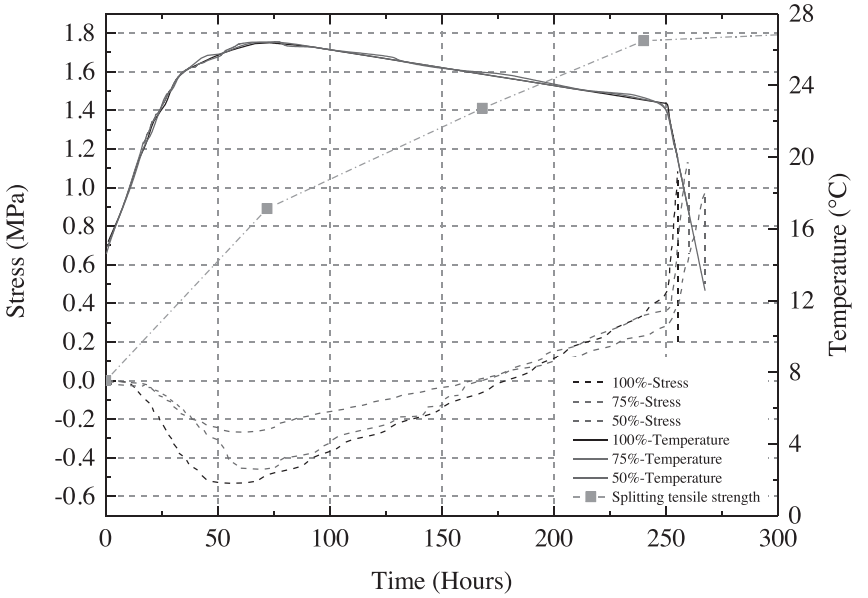

(b)

Figure 7. Evolutions of concrete restrained stress with a cooling rate of (a) 1.0°C/d-0.39°C/h; (b) 0.5°C/d-0.6°C/h.

NUMERICAL ANALYSIS OF CONCRETE RESTRAINED IN TSTM

In this section, two numerical analyses of concrete restrained stress in TSTM, namely 1D and 3D program, were conducted to reproduce and verify experimental results. All numerical analyses were based on the same material parameters obtained from experimental tests.

Based on experimental results, cracking was assumed to occur when restrained stress of concrete reached 65% of splitting tensile strength.

1D program using Matlab

For a restrained concrete, the evolution of stress can be calculated by using an integral form equation, as shown in Eq. (5).

$$\sigma = \int_0^t R(t, t')[d\varepsilon^0(t') - d\varepsilon(t')] \quad (5)$$

where $R(t,t')$ is the relaxation modulus; $d\varepsilon^0(t')$ is the free deformation; $d\varepsilon(t')$ is the residual deformation.

Since the acquirement of relaxation modulus needs complex computation by solving the Volterra integral equation (Neville, 1983), several methods have been developed to calculate restrained stress with creep compliance or creep coefficient, such as effective modulus method, age-adjusted effective modulus, and step-by-step method (Bažant, 1972a; Bažant, 1972b; Ghali et al., 2002). In this paper, the step-by-step method (as shown in Fig. 8) was employed.

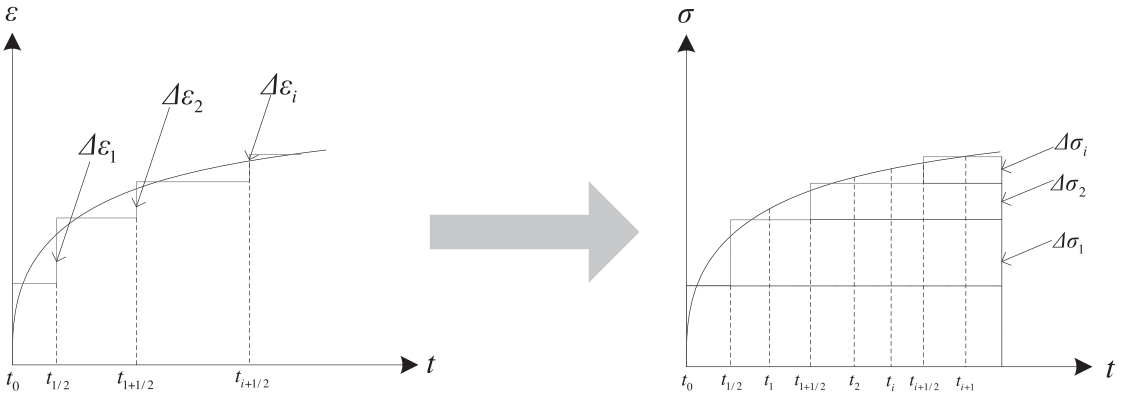

Figure 8. Step-by-step method of stress calculation (Ghali et al., 2002).

The stress increment $\Delta\sigma_i$ due to deformation increment $\Delta\varepsilon_i$ during the time period of $t_i \sim t_{i+1/2}$ can be expressed as (Tazawa, 1999).

$$(\Delta\sigma)_i = \frac{E(t_i)}{1+\varphi(t_{i+1/2},t_i)}\left\{\varepsilon(t_{i+1/2}) - \varepsilon^0(t_{i+1/2},t_0) - \sum_{j=1}^{i-1}\left[(\Delta\sigma)_j \frac{1+\varphi(t_{i+1/2},t_j)}{E(t_j)}\right]\right\} \quad (6)$$

where $E(t_i)$ is the elastic modulus at time t_i; $\varphi(t_{i+1/2},t_i)$ is the creep coefficient at time $t_{i+1/2}$; $\varepsilon(t_{i+1/2})$ is the residual deformation at time $t_{i+1/2}$; $\varepsilon^0(t_{i+1/2},t_0)$ is the total deformation during the time period of $t_0 \sim t_{i+1/2}$.

Then, the total stress can be expressed as (Tazawa, 1999).

$$\sigma(t_{i+1/2}) = \sum_{j=1}^{i}(\Delta\sigma)_j \quad (7)$$

Substituting Eq. (1) into Eq. (6), the stress increment of concrete in TSTM under an arbitrary restraint degree can be directly calculated, as shown in Eq. (8).

$$(\Delta\sigma)_i = \frac{E(t_i)}{1+\varphi(t_{i+1/2},t_i)}\left\{-\varepsilon^0(t_{i+1/2},t_0)\cdot\gamma_R - \sum_{j=1}^{i-1}\left[(\Delta\sigma)_j\frac{1+\varphi(t_{i+1/2},t_j)}{E(t_j)}\right]\right\} \quad (8)$$

To solve the step-by-step numerical formulation, the calculating algorithm was programmed with the Matlab software.

3D program using Midas

Numerical analysis of restrained stress of concrete in TSTM tests was also conducted using the commercial software Midas to simulate the time-dependent stress development. The thermal field of concrete was firstly calculated and acted as the external load for the subsequent stress analysis. The time increment during the calculation process was 2 hrs.

For the sake of simplification, only a quarter of concrete specimen and restraint frame was modelled in three dimensions for the finite element analysis, and the finite element size was selected as 5mm along three directions, as shown in Fig. 9. The concrete and restraint frame were modeled as an eight node isoparametric solid element. A central point was selected to investigate the representative stress evolution of concrete. All nodes in two symmetry planes of finite element model were fully restrained.

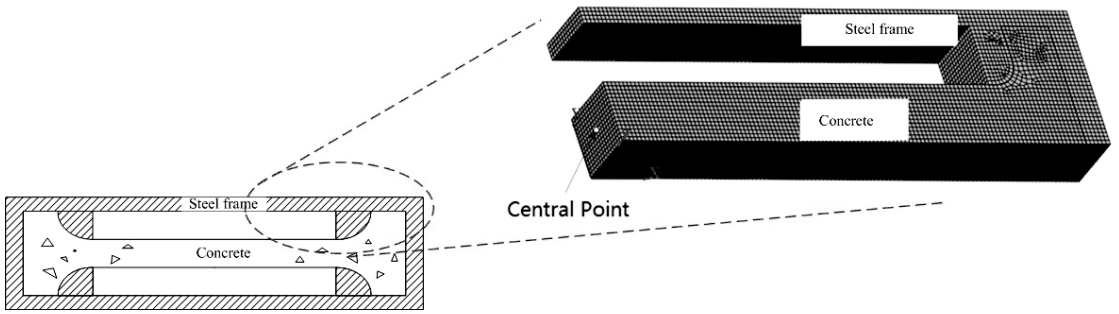

Figure 9. Finite element model (1/4 model).

The measured temperature evolution of concrete was implemented as a direct entry for numerical analysis. Meanwhile, it is assumed that no heat exchange occurred between the concrete and the steel frame and the temperature of restraint frame was kept at 14°C.

In order to simulate the restraint provided by the restraint frame, the following expression of restraint degree was used (ACI Committee 207, 1995; See et al., 2003):

$$\gamma_R = \frac{A_s E_s}{A_s E_s + A_c E_c} \quad (9)$$

where A_s and A_c are cross section area of restraint frame and concrete, respectively; E_s and E_c are elastic moduli of restraint frame and concrete, respectively.

The elastic modulus of steel frame can be obtained by rewriting Eq. (9):

$$E_s = \frac{\gamma_R A_c E_c}{(1-\gamma_R)A_s} \quad (10)$$

Then, an arbitrary restraint degree can be applied on the model by combining different material parameters of concrete and frame. In this paper, the dimension of restraint frame was constant, so the elastic modulus of restraint frame was deliberately designed using Eq. (10) for restrained stress analysis under various restraint degrees. It should be noted that creep behavior of concrete was not involved for evaluation of restraint degree.

Input numerical data

The input data for the stress analysis of TSTM tests are shown in Table 2.

Table 2. Input data for the concrete and the restraint frame in the numerical analysis.

Parameter	Concrete	Restraint frame
Elastic modulus	Eq. (3)	Eq. (10)
Splitting tensile strength	Eq. (4)	N/A
Poisson's ratio	0.20	0.30
Temperature history	Fig. 1	N/A
Thermal expansion coefficient	7.5×10^{-6}/°C	N/A
Casting temperature	14 ºC	N/A
Ambient temperature	14 ºC	14 °C

The Double Power Law (DPL) was used to model the creep behavior in the present work, as shown in Eq. (11) (Bažant and Osman, 1976).

$$\varphi=\varphi_0(t_0)^{-d}(t-t_0)^{p} \quad (11)$$

where φ_0 is ultimate creep coefficient of concrete; d and p are powers of creep function.

The input data for the creep behavior of concrete are shown in Table 3.

Table 3. Input data for the creep coefficient of concrete in the numerical analysis.

Parameter	Value
φ_0	1.2
d	0.2
p	0.1

Comparison with experimental results

Fig. 10 (a) and (b) show the comparison of experimental and 1D numerical results of restrained stress.

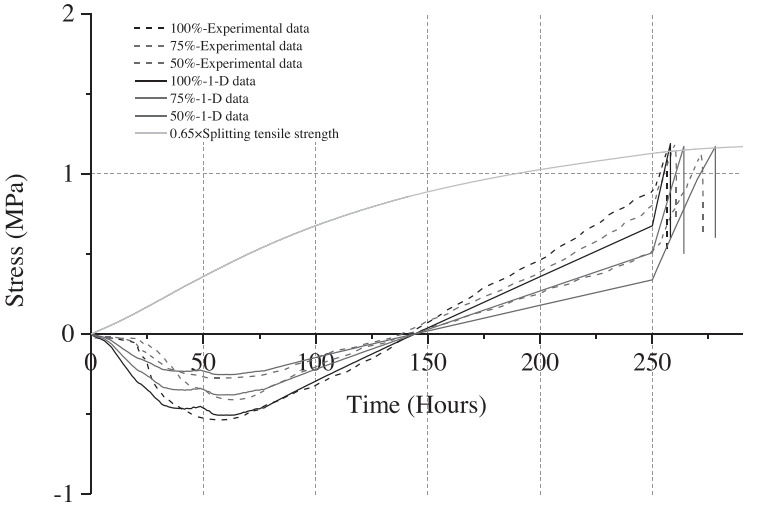

(a)

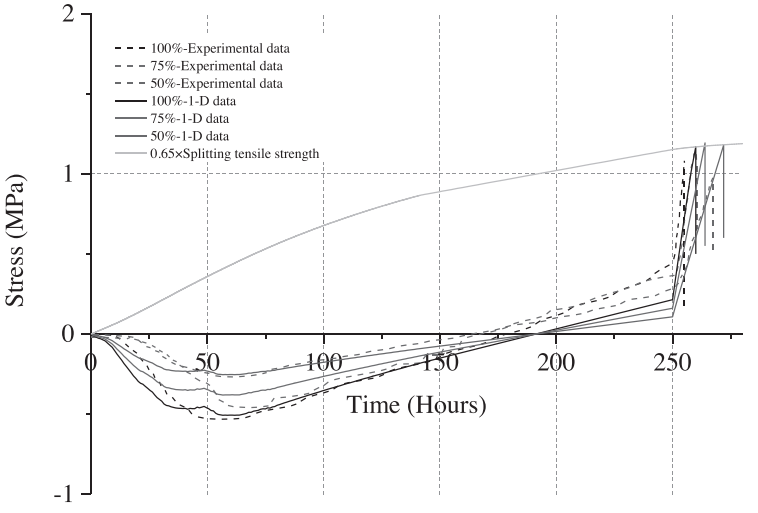

(b)

Figure 10. Comparison of experimental and 1D numerical restrained stresses: (a) 1.0°C/d-0.39°C/h; (b) 0.5°C/d-0.6°C/h.

In phase I, due to the rapid hydration process of cement, temperature gradually raised and reached 26.4 °C at 65 hours. Compressive stresses started to develop due to the restrained thermal deformation. As shown in Fig. 10(a), the maximum compressive stresses were -0.54MPa, -0.41MPa, and -0.28MPa for the restraint degrees of 100%, 75%, and 50%, respectively, which were similar with those values of the 1D numerical analysis results. In phase II, the temperature of specimens gradually decreased, and the compressive stress was accordingly reduced. At a critical point, the compressive stress converted to tensile stress and this point is called the "second-zero-stress" age and the corresponding temperature is named as "second-zero-stress" temperature (Emborg, 1989). Tensile stress developed faster when cooling rate of concrete increased during phase III and when it exceeded the tensile strength of concrete,

cracks occurred. The trends of compressive stress evolution in Fig. 10(b) were almost the same compared with those in Fig. 10(a); however, they were followed by slower compressive stress decrease periods, leading to later "second-zero-stress" ages.

Figs. 11 and 12 show the thermal field of concrete and restraint frame at age of 1h and 65h under the temperature history of 1.0°C/d-0.39°C/h. The temperature distribution of concrete was uniform along the cross section, which was similar to that of concrete specimen in TSTM tests. As can be seen in Fig. 12, the temperature of restraint frame was constant during the whole test period.

(a)

(b)

Figure 11. Thermal field of concrete at age of (a) 1h; (b) 65h.

(a)

(b)

Figure 12. Thermal field of restraint frame at age of (a) 1h; (b) 65h.

The temperature evolution of central point was extracted and compared with experimental data, as shown in Fig. 13. Good agreement was noted between the thermal field analysis and experimental results.

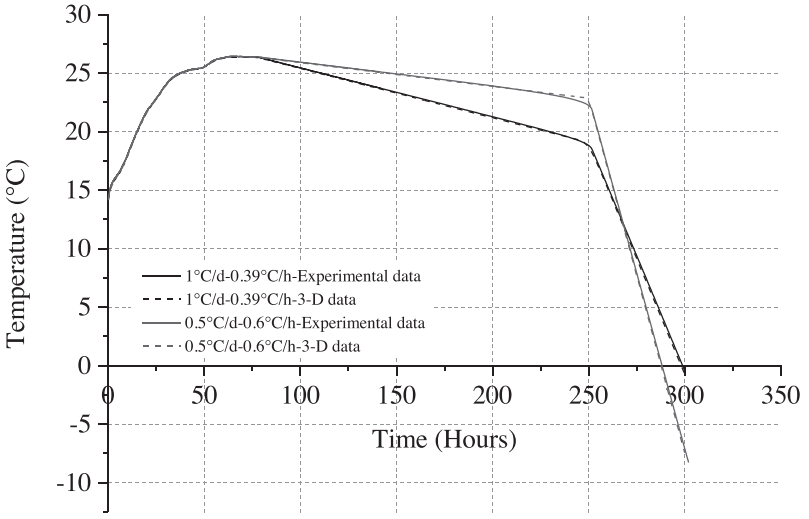

Figure 13. Comparison of experimental and numerical temperature of concrete.

Fig. 14 shows the comparison of experimental and 3D numerical restrained stresses. The comparison of stresses using two numerical methods has been presented in Fig.15. It can be seen from Fig. 14 that the numerical stress evolution trends with different restraint degrees were similar with experimental data; however, the specific values were different. The numerical compressive/tensile stresses were globally smaller than those of experimental values, leading to delayed cracking age. The reason for these differences will be discussed subsequently.

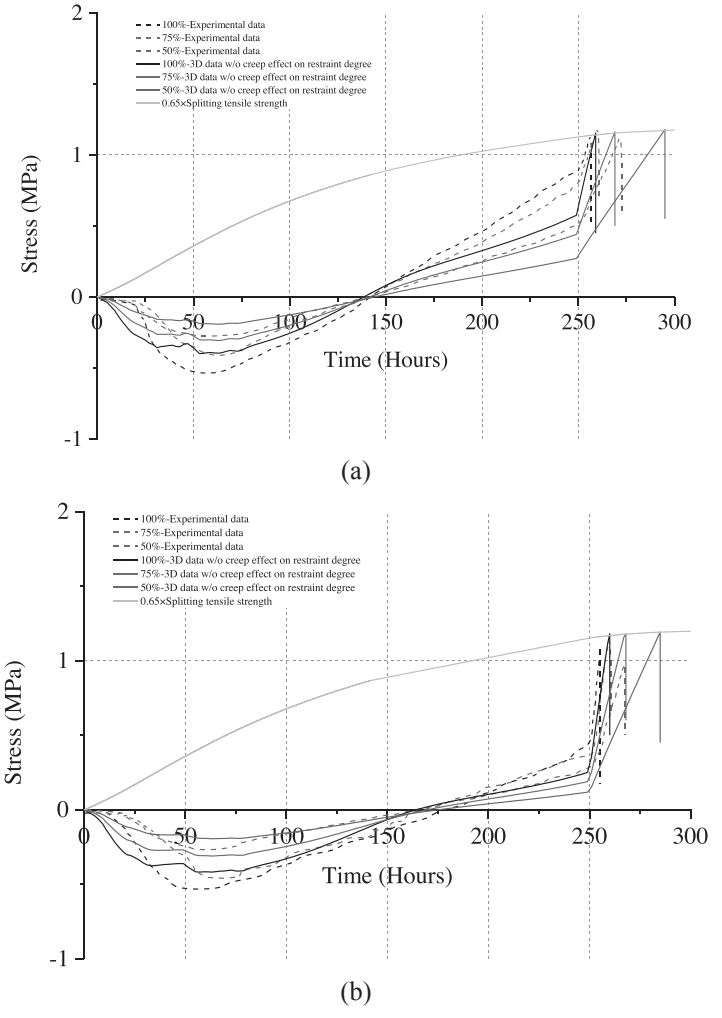

Figure 14. Comparison of experimental and 3D numerical stresses: (a) 1.0°C/d-0.39°C/h; (b) 0.5°C/d-0.6°C/h.

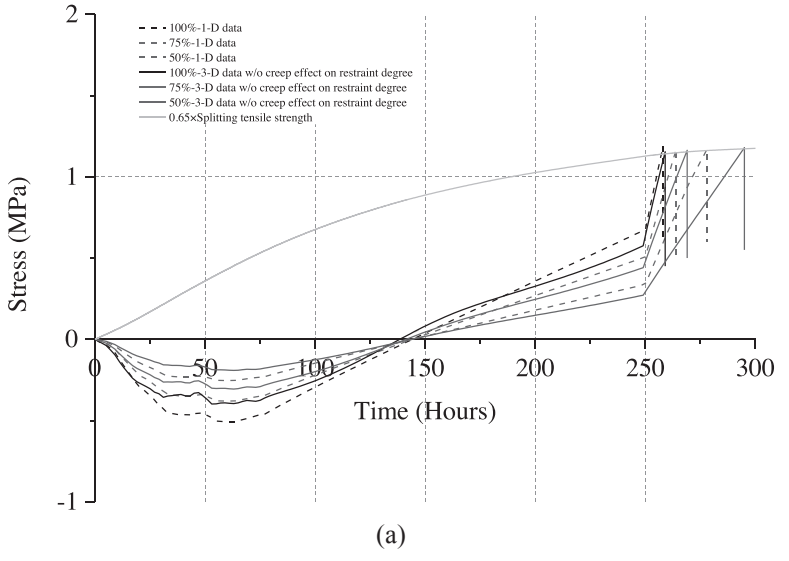

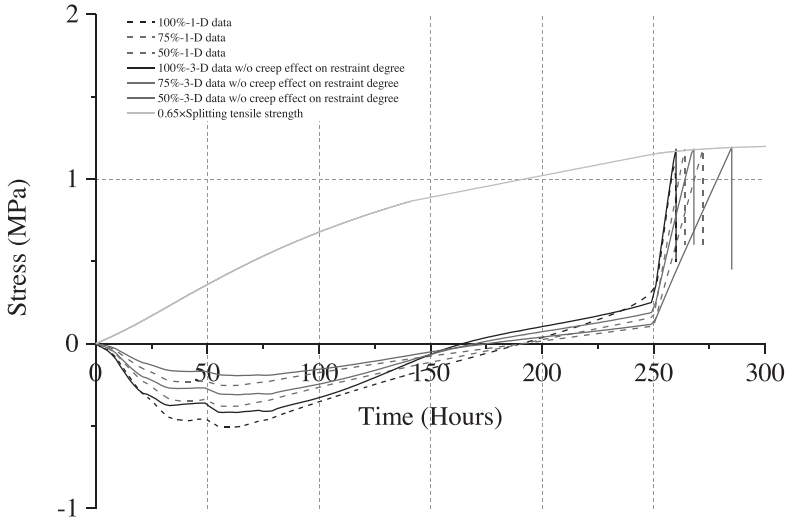

(b)

Figure 15. Comparison of 1D and 3D numerical stresses: (a) 1.0°C/d-0.39°C/h; (b) 0.5°C/d-0.6°C/h.

DISCUSSION

Table 4 presents measured and calculated temperature differences ΔT (the difference between maximum temperature and cracking temperature of concrete). The value in parenthesis refers to the ratios of temperature difference with the temperature history of 1.0°C /d-0.39°C/h to that of 0.5°C/d-0.6°C/h.

It can be seen from Table 4 that the temperature differences under the cooling rate of 1.0°C /d-0.39°C/h were globally larger than those under the cooling rate of 0.5°C/d-0.6°C/h. This phenomenon can be explained by the positive effect of strong creep capability and weak stiffness of concrete on reduction of restrained stress at early-age.

Table 4. Comparison of ΔT of experimental and numerical data.

	ΔT/°C					
Temperature history	1.0°C/d-0.39°C/h			0.5°C/d-0.6°C/h		
Restraint degree	100%	75%	50%	100%	75%	50%
Experiment	9.32	11.01	15.66	6.5	9.23	13.88
1D method	9.98(1.05)	12.73(1.07)	17.81(1.03)	9.5	11.9	17.3
3D method	10.77(1.13)	14.69(1.03)	24.85(1.01)	9.5	14.3	24.5

As expected, the magnitudes of temperature difference positively correlate with the restraint degree. With lower restraint degree, larger temperature difference will be needed to increase restrained stress of concrete, as well as to induce cracking of concrete.

It is shown in Fig.10 that, during the compressive stage, the curves of experimental and numerical data using the 1D method were very much alike, followed by lower restrained stress development of numerical data during the tensile stage. This phenomenon may be explained by the difference of compressive and tensile creep behavior of concrete (Ranaivomanana et al., 2013; Li et al., 2009; Rossi et al., 2012). Ranaivomanana et al. (2013) have pointed

out that the magnitude of tensile creep was smaller than compressive creep due to the impact of microcracking. Li et al. (2009) and Rossi et al. (2012) also had similar results. Since the models of creep coefficient under the compressive and tensile stages in the current research were the same, the calculated stresses during the tensile stage were lowered using the higher compressive creep property.

It is interesting to note from Fig. 14 that the values of calculated restrained stress using the 3D method were globally lower than those of the experimental data. Meanwhile, Table 4 also shows that the temperature differences calculated using the 3D method were larger than those of the experimental data, as well as those calculated using the 1D method. This difference can be attributed to the creep behavior of concrete.

Fig. 16 shows the strain evolution of concrete under restraint condition (expansion phase). The dotted lines represent original position of concrete, while solid lines represent actual position of concrete.

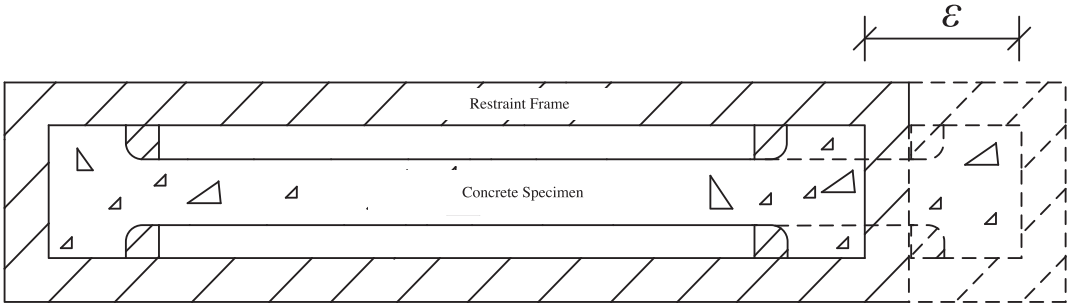

Figure 16. Strain of concrete under restraint condition.

Assuming that the actual strain of restraint frame is ε, the elastic strain of concrete ε^e can be calculated based on the principle of deformation compatibility and force equilibrium:

$$\varepsilon^e = \frac{\varepsilon E_S A_S}{E_C A_C} \tag{12}$$

If no creep strain occurred during the loading period, then the restraint degree provided by the restraint frame can be expressed using Eq. (1) as

$$\gamma_R = \frac{\varepsilon^e}{\varepsilon^e + \varepsilon} \tag{13}$$

Substituting Eq. (12) into Eq. (13), one can obtain the restraint degree expressed by Eq. (9).

In other words, the restraint degree expressed by the stiffness is comparable with that expressed by the deformation if creep effect is neglected.

In reality, creep deformation occurs when concrete experiences long-term loading (as shown in Fig. 17). If concrete creep effect is considered, then Eq. (9) should be rewritten as

$$\gamma_R = \frac{E_S A_S}{E_S A_S + \bar{E}_C A_C} \tag{14}$$

where $\bar{E}_C$ is an effective modulus of concrete incorporating creep behavior.

Figure 17. Creep of concrete beam under long-term loading (Miàs et al., 2013).

Clearly, the restraint degree expressed by Eq. (9) is lower compared with that expressed by Eq. (14) due to smaller concrete modulus, resulting in the fact that the calculated restrained stresses using the 3D method were globally lower than those using the 1D method (as shown in Fig. 15).

In order to take the creep effect into consideration, the age-adjusted effective modulus was adopted. This method was developed by Trost (1967), Dilger and Neville (1971), and Bazant (1972b). A reduced creep coefficient ($\chi\varphi(t)$) can be used to quantify the "ageing" effect of concrete. χ is called the ageing coefficient and can be taken as 0.8 for relaxation problems (Gilbert and Ranzi, 2011).

The age-adjusted effective modulus then can be calculated by Eq. (15)

$$\overline{E}_c = \frac{E_c}{1+\chi\varphi(t)} \tag{15}$$

Substituting Eq. (15) into (10), the elastic modulus of restraint frame was recalculated and used for restrained stress analysis. This process using the age-adjusted effective modulus (i.e., restraint degree with creep effect) can be considered as an improved 3D method.

Fig. 18 shows the comparison between the measured stresses and the calculated results using the improved 3D method and Table 5 presents measured and calculated temperature differences ΔT using the improved 3D method. The value in parenthesis refers to the ratio of temperature difference with the temperature history of 1.0°C/d-0.39°C/h to that of 0.5°C/d-0.6°C/h.

Table 5. Comparison of ΔT of experimental and improved 3D numerical data.

	ΔT/°C					
Temperature history	1.0°C/d-0.39°C/h			0.5°C/d-0.6°C/h		
Restraint degree	100%	75%	50%	100%	75%	50%
Experiment	9.32	11.01	15.66	6.5	9.23	13.88
1D method	9.98(1.05)	12.73(1.07)	17.81(1.03)	9.5	11.9	17.3
3D method	10.77(1.13)	14.69(1.03)	24.85(1.01)	9.5	14.3	24.5
Improved 3D method	9.59(1.16)	11.16(1.04)	15.86(1.02)	8.3	10.7	15.5

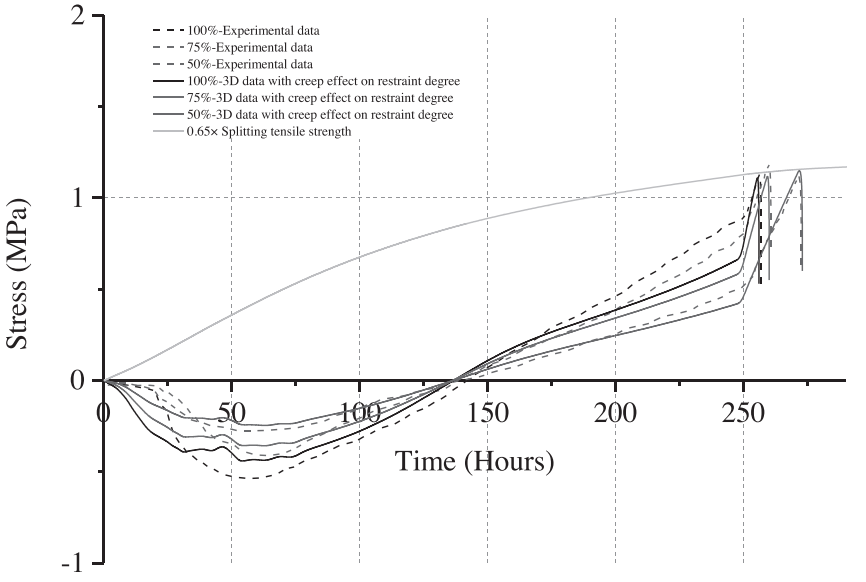

(a)

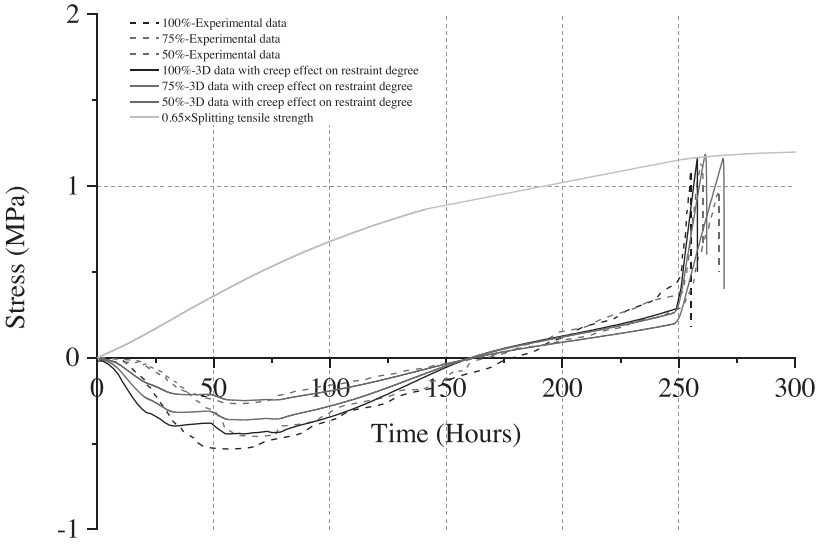

(b)

Figure 18. Comparison of experimental and improved 3D numerical stresses: (a) 1.0°C/d-0.39°C/h; (b) 0.5°C/d-0.6°C/h.

It can be seen that numerical results using the improved 3D method were closer to those of the experimental data. The aforementioned effect of creep behavior on restraint degree has been confirmed.

The optimally approximated relationship between the restraint degree and the temperature difference obtained from the improved 3D method can be expressed by Eq. (16), as shown in Fig. 19.

$$y = ax^b \tag{16}$$

where a and b are constants, determined from numerical data.

The values of *a* under the cooling rate history of 1.0 °C/d-0.39 °C/h and 0.5 °C/d-0.6 °C/h are 9.3 and 8.27, respectively. The values of *b* under the cooling rate history of 1.0 °C/d-0.39 °C/h and 0.5 °C/d-0.6 °C/h are -0.76 and -0.9, respectively.

It should be noted that Eq. (16) is just empirical, but helpful for engineers to easily evaluate cracking potential of concrete structures.

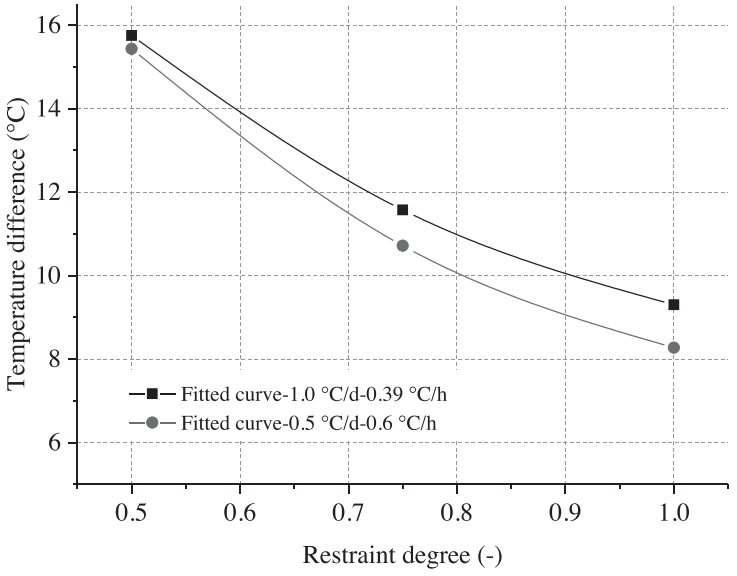

Figure 19. The relationships between the temperature difference and the restraint degree based on the improved 3D method.

CONCLUSIONS

In this paper, the effect of temperature history and external restraint degree (e.g., a RC wall restrained by a foundation or adjoining concrete structures) on restrained stress and cracking behavior of concrete was numerically investigated using two different analytical methods. The following conclusions can be drawn:

(1) With lower restraint degree, larger temperature difference will be needed to increase restrained stress of concrete, as well as to induce cracking of concrete. The experimental temperature differences of concrete increased from 9.32 °C to 15.66 °C when restraint degree changed from 100% to 50% under the temperature history of 1.0 °C/d-0.39 °C/h, which were consistent with numerical results using 1D and 3D method. For practice, methods for lowering restraint degree (e.g., shorter casting time interval and smaller Length/Height ratio) are beneficial for preventing concrete structures from bearing high restraint condition.

(2) The experimental temperature differences of concrete increased from 6.6 °C to 9.32 °C and 13.88°C to 15.66 °C when temperature history changed from 0.5 °C/d-0.6 °C/h to 1.0 °C/d-0.39 °C/h for 100% and 50% restraint degree, respectively. Increasing cooling rate at early-age reduced tensile stress and hence increased the allowed temperature differences of concrete. It is suggested that cooling phase should be started on the massive concrete structure construction as early as possible to reduce restrained stress.

(3) Based on the experimental results, cracking occurred when restrained stress of concrete reached 65% of splitting tensile strength. For concrete structures under long-term loading, the deterioration of concrete strength should be considered for cracking potential evaluation.

(4) A simplified relationship between the external restraint degree and the allowed temperature difference is developed,

which help engineers approximately estimate the cracking potential in massive concrete structures without going through the complex calculation.

(5) Both the 1D and 3D numerical analyses of restrained stress evolution in TSTM tests showed a similar trend with experimental data. The values of restraint degree based on elastic stiffness method were lower than those incorporating creep behavior, resulting in the fact that the allowed temperature differences were correspondingly 12%~56% higher than those incorporating creep behavior. Ignoring the effect of creep on restraint degree may underestimate the cracking potential of concrete.

ACKNOWLEDGMENT

The authors would like to acknowledge the support provided by the National Key R&D Program of China (Grant Nos. 2018YFC0406700, 2016YFB0201000), the National Natural Science Foundation of China (Grant Nos. 51579252, 51439005, and 51779277), the Special Scientific Fund sponsored by IWHR for Department of Structures and Materials (Grant Nos. SS0145B612017, SS0145B712017), the Special Scientific Research Project of the State Key Laboratory of Simulation and Regulation of Water Cycle in River Basin of IWHR (Grant No. SS0112B102016), the Special Scientific Research Project of the China Institute of Water Resources and Hydropower Research (Grant No. SS0145B392016), and the National Key Basic Research Program of China (Grant Nos. 2013CB036406, 2013CB035904). Support provided by China Three Gorges Corporation research project (Grant No. WDD/0428) is also gratefully acknowledged.

REFERENCES

ACI Committee 207. 1995. Effect of Restraint, Volume Change, and Reinforcement on Cracking of Mass Concrete (207.2R-95), Farmington Hills, Michigan.

Altoubat, S., Badran, D., Junaid, M.T. & Leblouba, M. 2016. Restrained shrinkage behavior of self-compacting concrete containing ground-granulated blast-furnace slag. Construction and Building Materials, **129**: 98-105.

Altoubat, S., Junaid, M.T., Leblouba, M. & Badran, D. 2017. Effectiveness of fly ash on the restrained shrinkage cracking resistance of self-compacting concrete. Cement and Concrete Composite, **79**: 9-20.

Amin, M.N., Kim, J.S., Lee, Y. & Kim, J.K. 2009. Simulation of the thermal stress in mass concrete using a thermal stress measuring device. Cement and Concrete Research, **39**(3): 154-164.

Bažant, Z.P. & Osman, E. 1976. Double power law for basic creep of concrete. Materials and Structures, **9**(1): 3-11.

Bažant, Z.P. 1972a. Numerical determination of long-range stress history from strain history in concrete. Materials and Structures, **5**(3):135-141.

Bažant, Z.P. 1972b. Prediction of concrete creep effects using age-adjusted effective modulus method. ACI Journal, **69**: 212-217.

Breitenbücher, R. 1990. Investigation of thermal cracking with the cracking-frame. Materials and Structures, **23**(3): 172-177.

China Standards. GB/T50081. 2002. Test standards and methods for mechanical properties of normal concrete. Beijing: People's Republic of China.

Dilger, W. & Neville, A.M. 1971. Method of creep analysis of structural members. ACI Journal, **27**: 349–372.

Emborg, M. 1989. Thermal stresses in concrete structures at early ages (Ph.D. thesis). Luleå University, Luleå, Sweden.

Fan, W.J., Wang, X.Y. & Park, K.B. 2015. Evaluation of the chemical and mechanical properties of hardening high-calcium fly ash blended concrete. Materials, **8**(9): 5933-5952.

Ghali, A., Favre, R. & Elbadry, M. 2002. Concrete structures: stresses and deformations (3rd Edition). E&FN Spon, London.

Gilbert, R.I. & Ranzi, G. 2011. Time-Dependent Behaviour of Concrete Structures. Spon Press, London.

Hossain, A.B. & Weiss, J. 2004. Assessing residual stress development and stress relaxation in restrained concrete ring specimens. Cement and Concrete Composite, **26**(5): 531-540.

Khan, I., Castel, A. & Gilbert, R.I. 2017. Effects of fly ash on early-age properties and cracking of concrete. ACI Material Journal, **114**(4): 673-681.

Kovler, K. & Bentur, A. 2009. Cracking sensitivity of normal-and high-strength concretes. ACI Material Journal, **106**(6): 537-542.

Kovler, K. 1994. Testing system for determining the mechanical behavior of early age concrete under restrained and free uniaxial shrinkage. Materials and Structures, **27**(6): 324-330.

Lee, H.K., Lee, K.M. & Kim, B.G. 2003. Autogenous shrinkage of high-performance concrete containing fly ash. Magazine of Concrete Research, **55**(6): 507-515.

Li, K., Ju, Y., Han, J. & Zhou, C. 2009. Early-age stress analysis of a concrete diaphragm wall through tensile creep modeling. Materials and Structures, **42**(7): 923-935.

Lin, Z.H. 2006. Quantitative evaluation of the effectiveness of expansive concrete as a countermeasure for thermal cracking and the development of its practical application (Ph.D. thesis). University of Tokyo, Tokyo, Japan.

Miàs, C., Torres L., Turon, A. & Barris, C. 2013. Experimental study of immediate and time-dependent deflections of GFRP reinforced concrete beams. Composite Structures, **96**: 279-285.

Neville, A.M., Dilger, W.H. & Brooks, J.J. 1983. Creep of plain and structural concrete. Construction Press, New York.

Ranaivomanana, N., Multon, S. & Turatsinze, A. 2013. Tensile, compressive and flexural basic creep of concrete at different stress levels. Cement and Concrete Research, **52**(10): 1-10.

Rossi, P., Tailhan, J.L., Le Maou, F., Gaillet, L. & Martin, E. 2012. Basic creep behavior of concretes investigation of the physical mechanisms by using acoustic emission. Cement and Concrete Research, **42**(1): 61-73.

See, H.T., Attiogbe, E.K. & Miltenberger, M.A. 2003. Shrinkage cracking characteristics of concrete using ring specimens. ACI Material Journal, **100**(3): 239-245.

Shi, N.N., Ouyang, J.S., Zhang, R.X. & Huang, D.H. 2014. Experimental study on early-age crack of mass concrete under the controlled temperature history. Advances in Materials Science and Engineering, **2014**: 1-10.

Springenschmid, R., Breitenbucher, R. & Mangold, M. 1994. Development of the cracking frame and the temperature-stress testing machine, In Thermal Cracking in Concrete at Early Ages, E & FN Spon, London, pp.137-144.

Tazawa, E. 1999. Autogenous Shrinkage of Concrete. In Proceedings of the International Workshop organized by the JCI (Japan Concrete Institute), E & FN Spon, London.

Trost, H. 1967. Auswirkungen des Superpositionsprinzips auf Kriech- und Relaxations Probleme bei Beton und Spannbeton. Beton- und Stahlbetonbau, **62**(10): 230-238, 261-269.

Wang, X.F., Fang, C., Kuang, W.Q., Li, D.W., Han, N.X. & Xing, F. 2017. Experimental study on early cracking sensitivity of lightweight aggregate concrete. Construction and Building Materials, **136**: 173-183.

Wang, Z., Liu, Y., Zhang, G. & Hou, W. 2015. Schematic study on temperature control and crack prevention during spillway tunnel concreting period. Materials and Structures, **48**(11): 3517-3525.

Zhang, T. & Qin, W.Z. 2006. Tensile creep due to restraining stresses in high-strength concrete at early ages Cement and Concrete Research, **36**(3): 584-591.

Zhu, B.F. 2013. Thermal stresses and temperature control of mass concrete. Oxford: Butterworth-Heinemann.